# Isothermal Crystallization Study on a Biodegradable Segmented Copolymer Constituted by Glycolide and Trimethylene Carbonate Units

**Elena Díaz-Celorio, Lourdes Franco, Jordi Puiggalí**

*Departament d'Enginyeria Química, Universitat Politècnica de Catalunya, E-08028 Barcelona, Spain*

Received 9 July 2009; accepted 5 October 2009
DOI 10.1002/app.31554
Published online 1 December 2009 in Wiley InterScience (www.interscience.wiley.com).

**ABSTRACT:** The isothermal crystallization behavior of a segmented copolymer constituted by hard blocks of polyglycolide and soft segments derived from the copolymerization of glycolide and trimethylene carbonate was investigated. This polymer has applied relevance because it is one of the most widely used for bioabsorbable surgical sutures. Calorimetric, optical microscopy, and infrared techniques were combined to understand the thermal properties and the different factors that influence the crystallization process. Basically, only the hard blocks crystallized, although certain processing conditions allowed performing an additional crystallization associated with small lamellar domains of the soft segment. Crystallization from both the melt and the glass state rendered positive spherulites with a fibrillar texture. The observed unusual sign of birefringence was a consequence of the close packing structure of polyglycolide, which was also corroborated by electron diffraction patterns. Crystallization was characterized by an athermal nucleation, which allowed accurate estimation of the secondary nucleation parameter by using the calorimetric data only. Significant differences in the Avrami exponent (from 2.32 to 1.45) were found between the cold and hot isothermal crystallizations. The stronger geometric constraints observed in the crystallization from the glass state were also corroborated by FTIR analyses. © 2009 Wiley Periodicals, Inc. J Appl Polym Sci 116: 577–589, 2010

**Key words:** polyesters; polyglycolide; surgical sutures; trimethylene carbonate; crystallization kinetics

## INTRODUCTION

Polyglycolide is a semicrystalline, biodegradable polymer that corresponds to the simplest of linear aliphatic polyesters derived from hydroxy acid units. It has been mainly applied as a bioabsorbable suture,[1] although uses as cell scaffolds, pins, screws for bone fixation, and drug delivery carriers have more recently been considered.[2,3] Polyglycolide degrades rapidly via hydrolysis, thus limiting applications when some specific properties are needed, for example, strength retention over a prolonged period of time. Furthermore, the low flexibility of polyglycolide requires processing in multifilament form when used as a suture. Problems like tissue drag and bacterial growth in wounds become enhanced. In this sense, copolymerization with more hydrophobic monomers such as ε-caprolactone and trimethylene carbonate (TMC) appears as a good alternative to tune material properties. Moreover, TMC is considered an ideal softening component for high-modulus polymers.[4]

Properties of materials depend on chemical composition, crystallinity, molecular weight, molecular orientation, and morphology. Several studies concerning these appear relevant for polymers used as biomaterials and based on glycolide units.[5–7] In this way, it has been demonstrated that mobile regions in polyglycolide and its copolymers are crucial for determining their ultimate mechanical and degradative properties.[8,9] Investigations on the crystallinity of constituent blocks and microdomain structures have focused attention on copolymers having at least one crystallizable block.

Maxon™ (Syneture), which was introduced in 1985 as a monofilament suture, is prepared by ring-opening copolymerization of glycolide (GL) and TMC, the final composition being defined by a 67.5 wt % (63 mol %) of glycolide.[10] Synthesis occurs in two steps, where a middle soft segment constituted by a theoretically random distribution of the above monomers is first produced using a glycolide feed molar ratio of 12%. Next, hard segments basically composed of glycolide units are incorporated, giving rise to the two end blocks of the copolymer (Scheme 1). The ratio, $x$, between soft and hard segments is close to 0.42 considering a simple balance for the

*Correspondence to:* J. Puiggalí (jordi.puiggali@upc.es).
Contract grant sponsors: CICYT and FEDER; contract grant number: MAT 2006-02406.

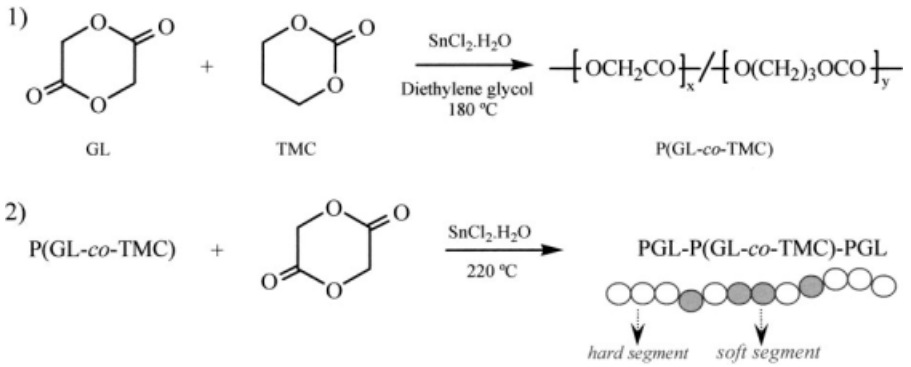


**Scheme 1** Two step synthesis of PGL-P(GL-*co*-TMC)-PGL.

glycolide units ($0.63 = (1 - x) + 0.12\ x$). This copolymer is hereafter called PGL-P(GL-*co*-TMC)-PGL to emphasize its segmented nature.

PGL-P(GL-*co*-TMC)-PGL has crystallizable glycolide blocks and a theoretically amorphous segment because of its statistical monomer distribution. The final microdomain structure should depend on the length ratio between these regular and irregular segments as well as on their miscibility. Note that a microphase separation could occur during cooling from the melt or heating from the glass state, respectively, when the central segment, rich in TMC units, becomes nonmiscible with the polyglycolide hard segments. Also, the soft segment may partially crystallize during the drawing step to which the extruded monofilament is subjected to increase its mechanical performance.

PGL-P(GL-*co*-TMC)-PGL appears as an interesting system because of its commercial application and use as the starting point in the analysis of related systems with a more complex constitution. Other polymers such as Monosyn™ (B. BRAUN Surgical) and Caprosyn™ (Syneture) are clear examples of sutures with soft segments constituted by three (glycolide, TMC, and ε-caprolactone) and four components (glycolide, TMC, ε-caprolactone, and lactide), respectively. This work is focused on the crystallization study under isothermal conditions by comparing the kinetic information obtained by DSC, optical microscopy, and infrared techniques.

## EXPERIMENTAL

### Materials

Commercially available sutures of PGL-P(GL-*co*-TMC)-PGL (Maxon™) and polyglycolide (Safil™) were purchased from Tyco Healthcare and B. BRAUN Surgical S.A., respectively. Weight-average molecular weight of Maxon™ samples was 95,000, as determined by GPC from 1,1,1,3,3,3-hexafluroisopropanol solutions and using poly(methyl methacrylate) standards.

### Measurements

Calorimetric data were obtained by differential scanning calorimetry with a TA Instruments Q100 series with $T_{zero}$ technology and equipped with a refrigerated cooling system operating at temperatures from −90°C to 550°C. Experiments were conducted under a flow of dry nitrogen with a sample weight of ~5 mg, and calibration was performed with indium. $T_{zero}$ calibration required two experiments: the first was performed without samples, whereas sapphire disks were used in the second.

The spherulite growth rate was determined by optical microscopy using a Zeiss Axioskop 40 Pol light polarizing microscope equipped with a Linkam temperature control system configured by a THMS 600 heating and freezing stage connected to a LNP 94 liquid nitrogen cooling system. Spherulites were grown from homogeneous melt-crystallized thin films produced by melting 1 mg of the polymer over microscope slides. Next, small sections of these films were pressed or smeared between two cover slides and inserted in the hot stage. The thicknesses of the squeezed samples were in all cases close to 10 μm. Samples were kept at 215°C (~10°C above the polymer melting point of 202°C) for 5 min to wipe sample history effects. For hot crystallization experiments, these samples were then quickly cooled to the selected crystallization temperature. For cold crystallization experiments, the above melted samples were quenched in liquid nitrogen and then quickly heated to the selected crystallization temperature. The radius of the growing spherulites was monitored during crystallization by taking micrographs with a Zeiss AxiosCam MRC5 digital camera at appropriate time intervals. A first-order red tint plate was used to determine the sign of spherulite birefringence under crossed polarizers.

A Philips TECNAI 10 electron microscope was used and operated at 80 and 100 kV for bright field and electron diffraction modes, respectively. Bright field micrographs were taken with a SIS MegaView II digital camera. Selected area electron diffraction patterns were recorded on Maco EM films. The patterns were internally calibrated with gold ($d_{111}$ = 0.235 nm). Spherulites were grown from homogeneous melt-crystallized thin films of PGL-P(GL-*co*-TMC)-PGL at 170°C, which were produced by evaporation of a dilute solution of the polymer in hexafluoroisopropanol.

Infrared absorption spectra were recorded with a Fourier Transform FTIR 4100 Jasco spectrometer in the 4000–600 $cm^{-1}$ range. A Specac model MKII Golden Gate attenuated total reflection (ATR) cell with a heated Diamond ATR Top-Plate, which can be used at up to 200°C, and a Series 4000 High-Stability Temperature Controller were also used.

## RESULTS AND DISCUSSION

### Thermal properties of PGL-P(GL-*co*-TMC)-PGL

The DSC heating scan of a commercial suture [Fig. 1(a)] showed a large endothermic peak near 200°C, which corresponded to the melting of polyglycolide hard segments and also a very small peak near 120°C. The latter probably corresponded to highly defective crystals, which might have formed either by crystallization under severe constraints or incorporation of comonomer impurities (i.e., TMC units). It is interesting to note that the high drawing ratio used to increase the modulus, and, in general, the mechanical properties of the final suture led to a crystallization that rendered this low temperature melting peak at 120°C. The subsequent cooling run from a melted sample [Fig. 1(b)] exhibited a single exothermic peak at 169°C, which delimited the range within which isothermal hot crystallization experiments could be performed (i.e., between 186 and 175°C). Interestingly, the heating run of a melt crystallized sample [Fig. 1(c)] only showed the single endothermic peak attributed to the polyglycolide hard segments, which means that the defective crystals did not form during the cooling process. The amorphous part should be mainly rich in TMC units, and consequently, a single glass transition temperature was observed at a relatively low value (6.1°C). Analysis of an amorphous sample obtained by quenching in liquid nitrogen [Fig. 1(d)] revealed a clearly different behavior. In this case, the amorphous phase was richer in glycolide units, and thus the glass transition temperature increased to 20°C. It is worth pointing out that in all cases, a single glass transition was observed although at variable temperatures ranging between those characteristic of polyglycolide (35–40°C) and polytrimethylene carbonate (−19°C), which is indicative of complete miscibility between soft and hard segments.

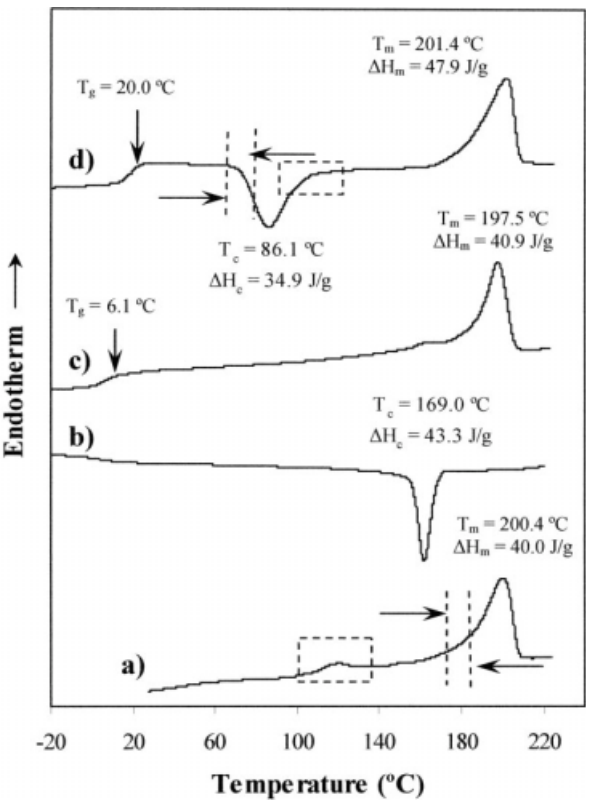


**Figure 1** DSC traces obtained with the segmented PGL-P(GL-*co*-TMC)-PGL sample during the heating run of the commercial suture (a), the cooling run after keeping the sample in the melt state for 5 min (b), the heating run of the hot crystallized sample (c), and the heating run of a quenched sample from the melt state (d). Dashed lines indicate the restricted intervals where DSC isothermal cold and hot crystallization experiments could be performed.

The heating scan of the quenched sample also showed a clear exothermic peak corresponding to cold crystallization. This peak has a very broad tail [dashed box in Fig. 1(d)] after reaching a temperature of 95°C, suggesting a complex process where crystallization and melting occurred practically simultaneously, as will be discussed later. It should be noted that only the endothermic peak attributed to the polyglycolide hard segments was observed. Figure 1(d) also illustrates the temperature range where the isothermal cold crystallization of the hard polyglycolide segments appears feasible.

Figure 2 shows the DSC exotherms of the PGL-P(GL-*co*-TMC)-PGL sample during cold and hot crystallization experiments at selected temperatures. The exothermic peak observed during the hot crystallization shifted to higher temperatures and became broader as the crystallization temperature was increased [Fig. 2(a)], whereas the opposite

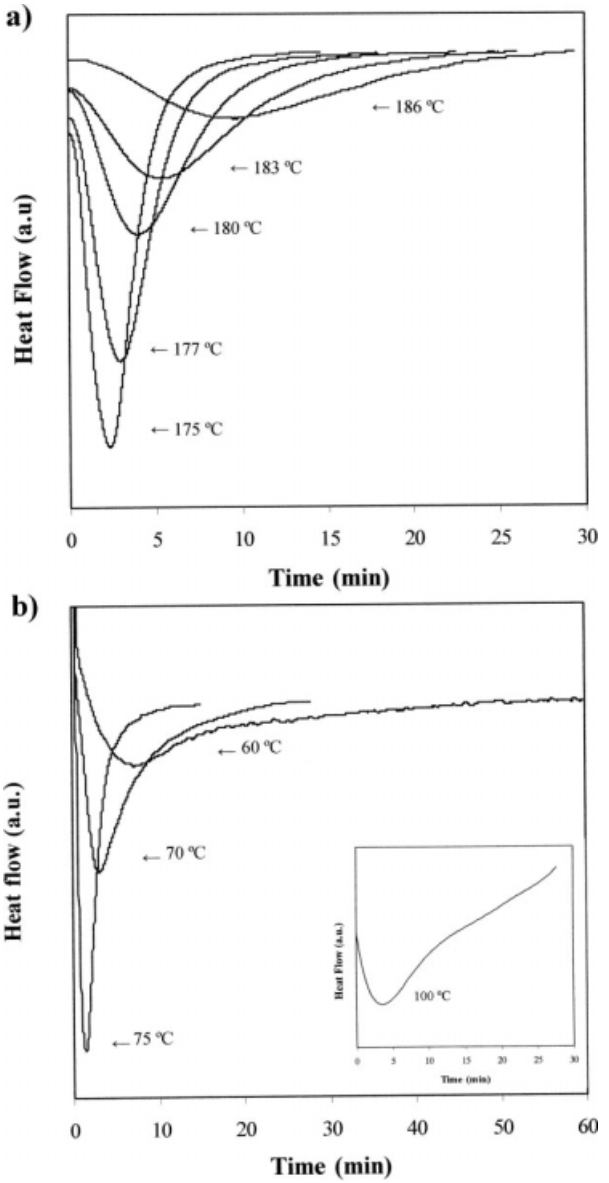


**Figure 2** (a) Exothermic DSC peaks corresponding to the hot isothermal crystallizations performed between 186 and 175°C (a) and the cold isothermal crystallizations performed between 60 and 75°C (b). Inset shows the small exothermic peak corresponding to a cold crystallization performed at 100°C after a previous crystallization at 75°C.

behavior was logically found for the cold crystallization [Fig. 2(b)]. Two well-differentiated cold crystallization processes occurred. The first took place at a low temperature (between 60 and 75°C) and was associated with the hard polyglycolide segments. The second was observed over a limited crystallization temperature range only (between 100 and 109°C) and appeared as a very broad exotherm with low melting enthalpy [inset in Fig. 2(b)]. This crystallization seemed to involve segments with poor glycolide content or short-length glycolide blocks.

A double melting peak was detected for samples isothermally crystallized from the melt, as shown in Figure 3(a). The first and second peak temperatures increased with crystallization temperature, $T_c$, as well as the relative area associated with the first peak. This behavior suggested the existence of two populations of lamellar crystals of different thickness. The first peak corresponded to more defective lamellae, whose reorganization/recrystallization process became more significant (i.e., the peak had a lower relative area) when crystals formed at lower temperatures. It is worth emphasizing that the second peak temperature also depended on the crystallization temperature as a clear shift was detected.

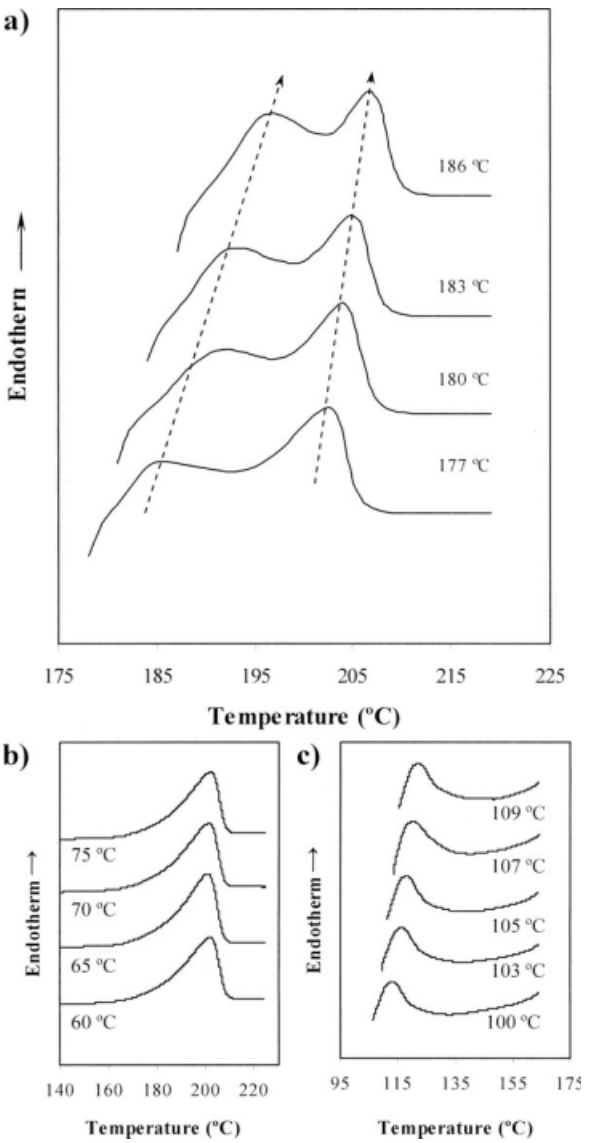


**Figure 3** DSC heating runs (20°C/min) of PGL-P(GL-*co*-TMC)-PGL samples isothermally crystallized at temperatures ranging from 177 to 186°C (a), from 60 to 75°C (b), and from 100 to 109°C (c).

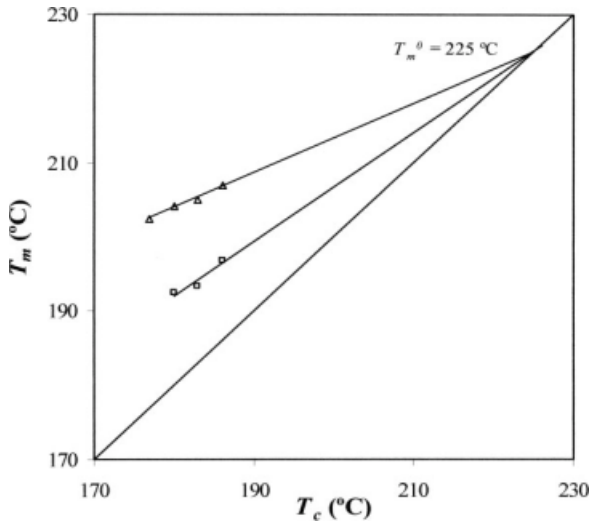


**Figure 4** Hoffman–Weeks plot of temperatures corresponding to endothermic melting peaks versus hot crystallization temperature. An equilibrium melting temperature close to 225°C was deduced.

Thus, the initial crystalline state determines the characteristics of reorganized lamellae.

To analyze the crystallization kinetics, it is necessary to determine the equilibrium melting point ($T_m^0$) of the PGL-P(GL-*co*-TMC)-PGL sample. One method is the Hoffman–Weeks approach[11] in which the experimental melting temperature ($T_m$) is plotted as a function of crystallization temperature ($T_c$) and extrapolated to the equilibrium conditions. These should be attained with an ideal infinite crystal, which according to the theory could only be obtained when samples were hypothetically crystallized at the same temperature as they melted. A theoretical equilibrium melting temperature of 225°C, which is close to the theoretical value reported for polyglycolide (229°C),[12] was graphically determined (Fig. 4) considering the data for the high-temperature melting crystals. A similar temperature was also inferred from the low-temperature melting peak. However, in this case, although overlapping of melt and recrystallization processes made it more difficult to obtain an accurate peak temperature value, an equilibrium melting temperature close to the previously reported value of 229°C was estimated.

Isothermal cold crystallizations performed in the 60–75°C temperature range gave rise to samples characterized by a single melting peak, which appeared at a practically constant temperature [202°C, as shown in Fig. 3(b)]. It is worth pointing out that this value is slightly lower than that found in the hot crystallization experiments. This peak should correspond to reorganized crystals formed during the heating scan because the initial crystals obtained at low temperatures appeared highly susceptible to recrystallization. Thus, the simultaneous melt/recrystallization process that undergoes the imperfect initial crystals is not reflected in the corresponding DSC traces. It should be pointed out that the melting temperature observed at a temperature close to 202°C suggests that reorganized crystals could not reach the degree of perfection/order attained when samples crystallized at high temperatures.

The heating run of samples isothermally crystallized first at 60–75°C and subsequently at 100–109°C

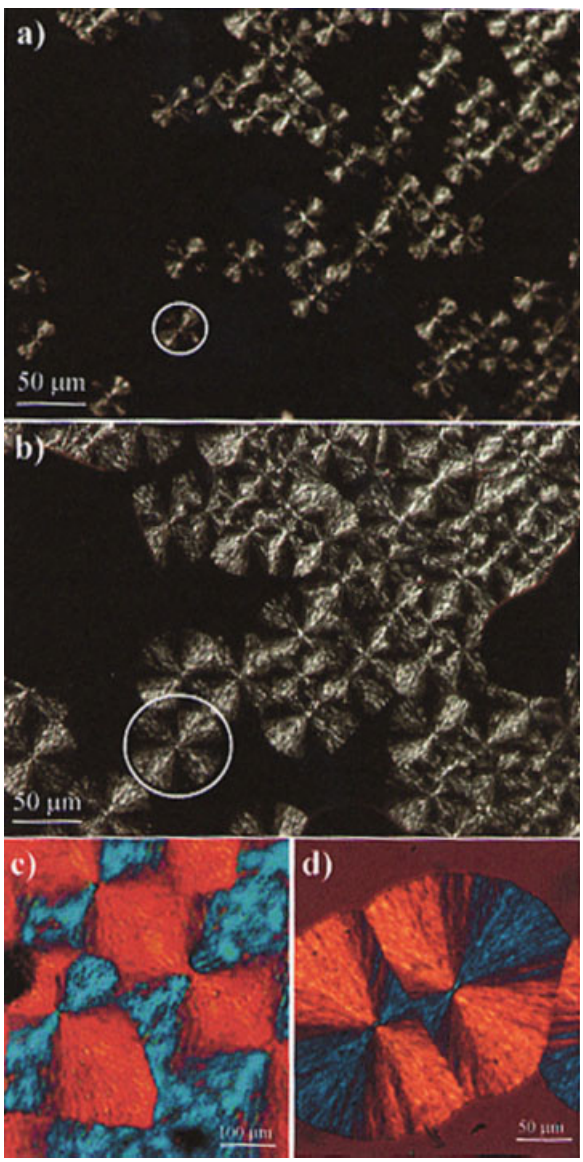


**Figure 5** Polarized optical micrographs showing spherulites of cold (a, b, c) and hot crystallized (d) PGL-P(GL-*co*-TMC)-PGL samples. Black and white micrographs correspond to samples crystallized at 80°C for 180 s (a) and 375 s (b). Micrographs of spherulites crystallized at 97 (c) and 175°C (d) taken using a first-order red tint plate at the end of the crystallization. [Color figure can be viewed in the online issue, which is available at www.interscience.wiley.com.]

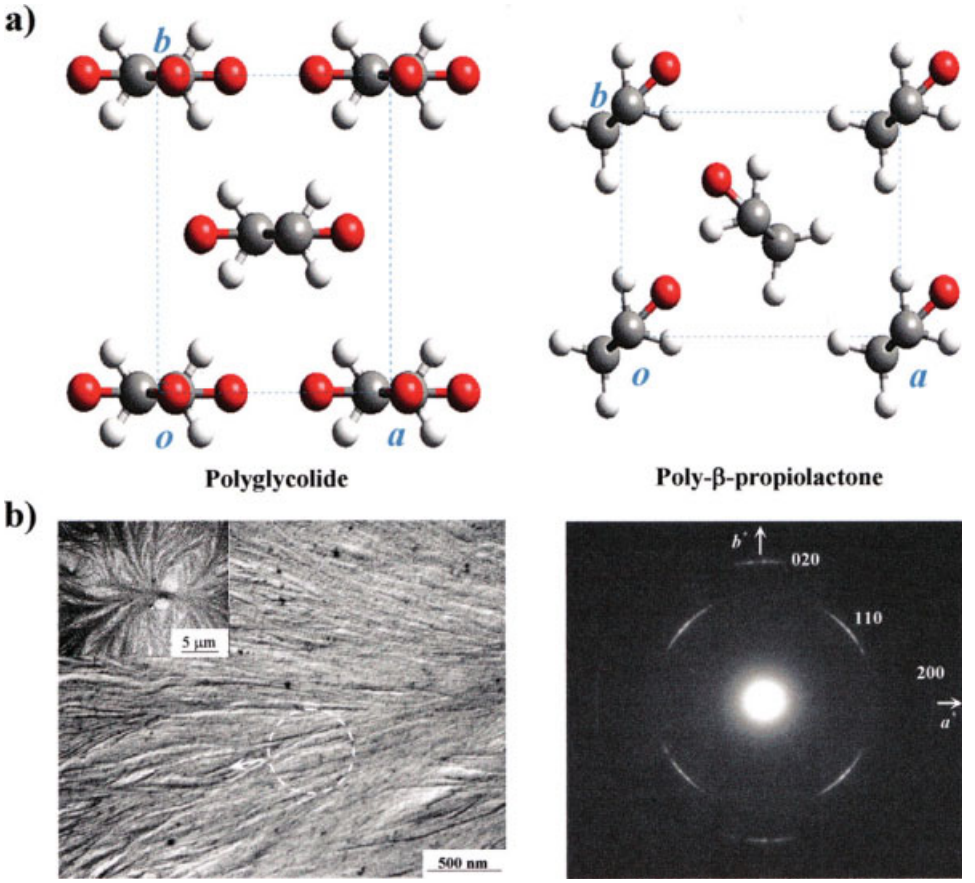


**Figure 6** (a) View parallel to the chain axis comparing the packing of polyglycolide[14] (left) and poly-β-propiolactone (right),[15] a polyester which has a zigzag conformation as well. Color code: hydrogen, white; carbon, gray; oxygen, red. (b) Transmission electron micrograph of a PGL-P(GL-*co*-TMC)-PGL spherulite crystallized at 170°C from a thin film prepared by evaporation of a diluted hexafluoroisopropanol solution. Inset shows the *hk*0 electron diffraction pattern of a thin spherulite zone. The *a** reciprocal axis is parallel to the spherulite radius. [Color figure can be viewed in the online issue, which is available at www.interscience.wiley.com.]

shows an additional endothermic peak at ~120°C, which corresponds to the peak observed in the first heating run of the commercial sutures. In fact, these manufactured samples are produced by a sequence that involves melt spinning, quenching, drawing, and annealing. Thus, their thermal properties (first scan in Fig. 1) must be in accordance with a cold crystallization process. Note, for example, that the high melting peak appeared at a temperature close to 200°C, in full agreement with the cold crystallization data.

The temperature of the new endotherm slightly increased again when the isothermal crystallization temperature did so. Application of the Hoffman and Weeks plot leads to an equilibrium melting temperature higher than 200°C, similar to that determined for polyglycolide, and consequently, still attributable to glycolide-rich segments. However, it is clear that this value cannot be accurately deduced because of both scarce experimental data and the implicit error associated with a high-temperature extrapolation value. The reduced $T_m$ values (e.g., 120°C) can be interpreted as a consequence of very thin lamellar domains crystallized under severe geometric constraints resulting from the main cold crystallization process. These small domains should correspond to the soft segment because similar experiments performed with polyglycolide (not shown) did not reveal the existence of the low temperature peak. In fact, the higher reactivity of glycolide with respect to the TMC ring may justify the existence of small glycolide blocks in the soft segment.

### Microscopy studies on the spherulitic morphology and crystallization kinetics of PGL-P(GL-*co*-TMC)-PGL

Polyesters usually crystallize into spherulites with negative birefringence and different textures, which can be fibrillar, banded, or double-banded depending on the polymer and the crystallization temperature.[13] PGL-P(GL-*co*-TMC)-PGL rendered highly positive birefringent spherulites during both cold and hot crystallization experiments. A fibrillar texture

with the Maltese cross was characteristic, as can be seen in the series of polarized optical micrographs (Fig. 5). Note that the sign of the birefringence is different from that usually observed in aliphatic polyesters. This is probably a consequence of the peculiar structure of polyglycolide, where molecules with a fully extended zigzag conformation form sheets parallel to the *ac* crystallographic plane [Fig. 6(a)].[14] Thus, the setting angle of the molecular segments is 0° or 180°, a value that differs from the angle of ±45° observed in other aliphatic polyesters with a planar zigzag conformation [Fig. 6(a)] and even in polyethylene, which can be considered as a model for samples with a large methylene/ester ratio in the repeat unit. Electron diffraction patterns of thin zones of PGL-P(GL-*co*-TMC)-PGL spherulites reveal that the *a* crystallographic axis was parallel oriented to the spherulite radius [Fig. 6(b)]. Reflections appear slightly arched and correspond to the 110 (0.399 nm), 020 (0.309 nm), and 200 (0.261 nm) reflections of an orthorhombic unit cell with $a = 0.522$ nm, $b = 0.619$ nm, and $c = 0.702$ nm. Note that reflections 100 and 010 could not be detected, in agreement with the extinction rule of the postulated $P2_12_12_1$ space group.

Optical properties of aliphatic polyamides have been extensively studied, revealing an interesting relationship with the molecular packing than may be useful in interpreting the peculiar characteristics of polyglycolide spherulites. It is well known that the structure of aliphatic polyamides (e.g., the α and β forms of nylon 66[16]) is defined by a stacking of sheets constituted by hydrogen-bonded molecules with a planar zigzag conformation. The azimuthal orientation of such molecules is determined by a setting angle close to 0° with respect to the hydrogen-bonding direction (i.e., the *a* crystallographic axis). These polyamides rendered positive birefringent spherulites when hydrogen bonds became aligned with the spherulite radius and negative when they became aligned in the tangential direction of the spherulites.[17,18] Thus, the positive sign of polyglycolide spherulites and the specific orientation of polyglycolide molecules seem to be in agreement with the reported data on aliphatic polyamides.

The cold and hot crystallizations of PGL-P(GL-*co*-TMC)-PGL were studied by optical microscopy in the range from 75 to 97°C and from 160 to 186°C, respectively, where spherulites with adequate dimensions formed. These reached diameters of 270 and 100 μm at crystallization temperatures close to 175 and 97°C, respectively. Larger dimensions were obtained in the hot crystallization experiments performed at temperatures sufficiently high to have a low nucleation rate compared with the crystal growth rate. This size decreased with decreasing crystallization temperature and reached a value close to 35 μm at 160°C. Average diameters close to 40 μm were measured at 75°C, allowing analysis of crystal growth up to this cold crystallization temperature.

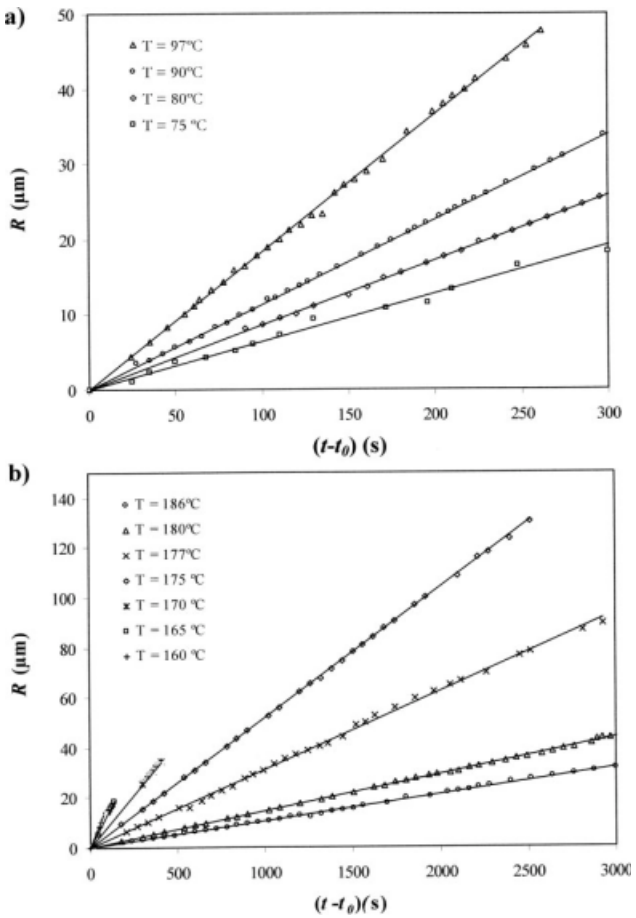


**Figure 7** Plots of the radius of PGL-P(GL-*co*-TMC)-PGL spherulites versus crystallization time for isothermal cold (a) and hot (b) crystallizations performed at temperatures ranging between 75–97°C and 160–186°C, respectively.

Spherulite radii grew linearly with time up to impingement within the studied temperature intervals (Fig. 7). The measured radial growth rates, *G*, vary from minimum values of 0.01 and 0.06 μm/s at 186 and 75°C, respectively, to maximum values close to 0.16 and 0.18 μm/s at 160 and 97°C, respectively.

Next, growth data are analyzed in terms of crystallization regimes because experimental data can be easily described by the mathematical expressions derived from the model of crystal growth and nucleation proposed by Lauritzen and Hoffman (LH).[19] It is nevertheless true that the physical meaning of the model may be questioned considering the new theories based on experimental evidence (e.g., the existence of a mesomorphic precursor phase before the development of a stable crystalline phase[20]) and different theoretical calculations.[21]

The radial growth rate (*G*) of polymer spherulites can then be calculated according the Hoffman and

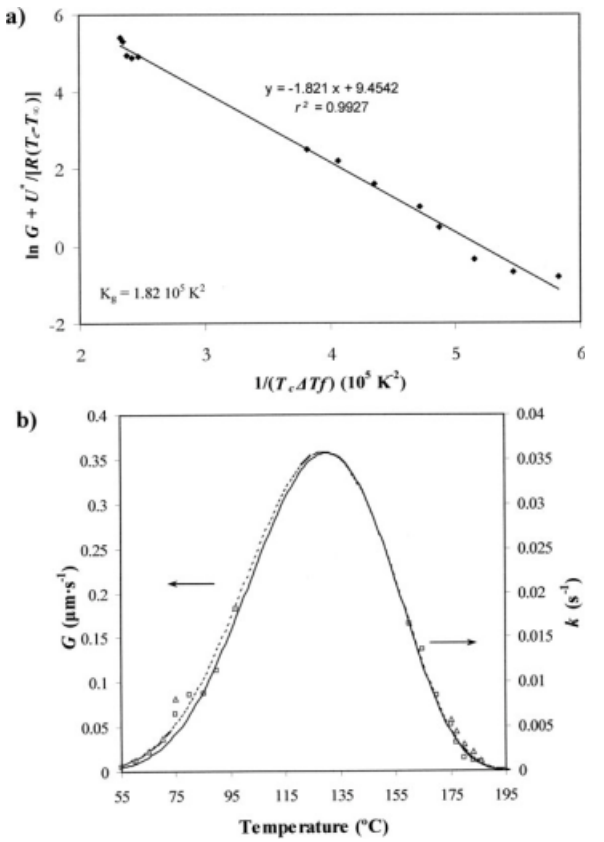


**Figure 8** (a) Plot of ln $G + U^*/R(T_c - T_\infty)$ versus $1/T_c(\Delta T)f$ to determine the $K_g$ nucleation parameter of PGL-P(GL-*co*-TMC)-PGL. Data from cold and hot crystallization experiments are represented. (b) Temperature dependence of the crystal growth rate (dashed line) and the overall crystallization rate (solid line) according to eqs. (1) and (4) and using the best fit parameters listed in the text. Experimental data, that is, crystal growth rates (□) and overall crystallization rate (△), are also shown for comparison.

Lauritzen equation[19]:

$$G = G_0 \exp[-U^*/(R(T_c - T_\infty))] \exp\left[-K_g/(T_c(\Delta T)f)\right], \quad (1)$$

where $G_0$ is a constant preexponential factor, $U^*$ represents the activation energy characteristic of the transport of crystallizing segments across the liquid-crystal interface, $T_\infty$ is a hypothetical temperature below which such motion ceases, $T_c$ is the crystallization temperature, $R$ is the gas constant, $K_g$ is the secondary nucleation parameter, $\Delta T$ is the degree of supercooling measured as $T_m^0 - T_c$, and $f$ is a correction factor accounting for the variation in the bulk melting enthalpy per unit volume with temperature ($f = 2T_c/(T_m^0 + T_c)$).

The sets of parameters most commonly used for $U^*$ and $T_\infty$ are those reported by Williams–Landel–Ferry[22] (WLF) ($U^* = 4120$ cal/mol and $T_\infty = T_g - 51.6$ K) and Suzuki and Kovacs[23] ($U^* = 1500$ cal/mol and $T_\infty = T_g - 30$ K).

Following LH plot, the experimental spherulitic growth rates of PGL-P(GL-*co*-TMC)-PGL were plotted as ln $G + U^*/R(T_c - T_\infty)$ versus $1/(T_c(\Delta T)f)$ [Fig. 8(a)]. The data fit well with a linear plot representative of a single crystallization regime if the $U^*$ and $T_\infty$ parameters took values of 1550 cal/mol and $T_g - 40$ K, respectively, which rendered the best linear regression coefficient ($r^2$: 0.9927). A nucleation parameter of $1.82 \times 10^5$ K$^2$ was derived from the slope of this linear plot.

Figure 8(b) shows that the bell-shaped curve calculated by eq. (1), the estimated $U^*$ and $T_\infty$ parameters, and the deduced values of $G_0$ and $K_g$ fit with the growth data obtained for the cold and hot crystallization experiments. The simulated curve shows that the maximum growth rate should be reached at a temperature of 130°C.

In addition to the crystal growth rate, the overall crystallization of a sample depends on primary nucleation, which may correspond to heterogeneous nuclei or homogeneous nuclei. In general, primary nucleation is a rather complex process as it depends on the crystallization temperature, density of heterogeneities, and presence/absence of nucleating agents.

The number of nuclei remained constant during crystallization for each isothermal experiment [e.g., Fig. 5(a,b)], suggesting athermal nucleation for the hot and cold crystallization experiments of PGL-P(GL-*co*-TMC)-PGL. It should be pointed out that all nuclei became active practically simultaneously for a given crystallization temperature, and a high degree of homogeneity in the spherulitic size was therefore observed at the end of the crystallization process. Figure 9 shows that the nucleation density increases

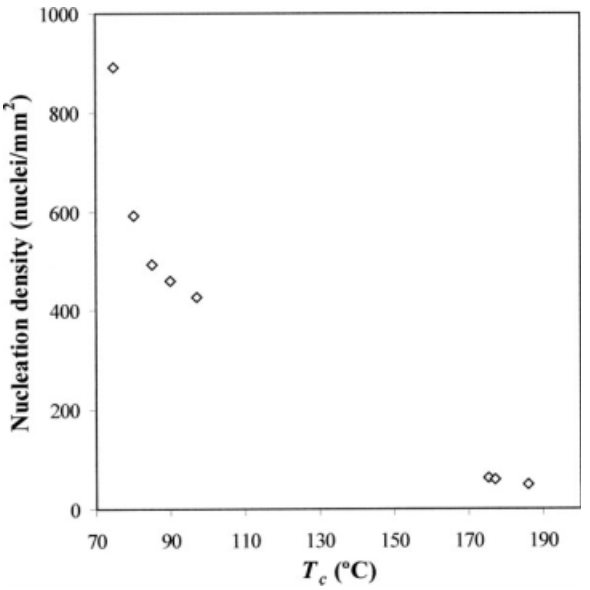


**Figure 9** Change in the nucleation density with isothermal crystallization temperature.

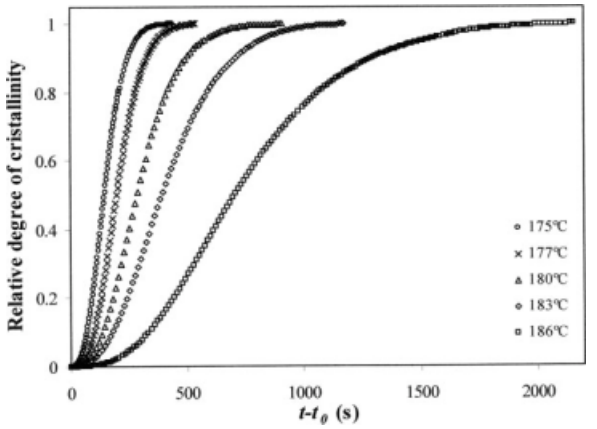


**Figure 10** Development of relative crystallinity over time for different isothermal crystallizations performed between 175 and 186°C.

with decreasing temperatures for both the melt- and glass-crystallized samples. The experimental data in Figure 9 suggest a single exponential dependence between the nucleation density and the crystallization temperature, which resulted in more active nuclei (i.e., more favorable thermodynamic conditions for nuclei generation) when this temperature progressively decreased. Note that the number of active nuclei is in general rather low, even at a lower temperature such as 80°C (i.e., 600 nuclei/mm$^2$).

### DSC calorimetric analysis of the isothermal crystallization of PGL-P(GL-*co*-TMC)-PGL

Kinetic calorimetric data are useful and complement the information obtained from microscopy studies as they allow determination of the overall crystallization kinetics, which depends on primary nucleation and crystal growth.

The time evolution of the relative degree of crystallinity, $\chi(t)$, was determined from hot and cold crystallization exotherms (Fig. 2) through the ratio area of the exotherm up to time $t$ divided by the total exotherm area, i.e.:

$$\chi(t) = \int_{t0}^{t} (dH/dt)dt \Big/ \int_{t0}^{\infty} (dH/dt)dt, \qquad (2)$$

where $dH/dt$ is the heat flow rate and $t_0$ the induction time. The development of crystallinity always showed a characteristic sigmoidal dependence on time, as plotted in Figure 10 for five hot crystallization experiments.

Kinetic crystallization data were analyzed assuming the well-known Avrami equation[24,25] for primary crystallization:

$$I - \chi(t) = \exp[-Z(t - t_0)^n], \qquad (3)$$

**TABLE I**
**Isothermal Crystallization Kinetic Parameters Deduced from DSC Experiments for the Segmented PGL-P(GL-*co*-TMC)-PGL Sample**

| $T_c$ (°C) | $n$ | $Z \times 10^6$ ($s^{-n}$) | $k \times 10^3$ ($s^{-1}$) | $\tau_{1/2}$ (s) |
|---|---|---|---|---|
| 60 | 1.44 | 65.86 | 1.23 | 620 |
| 65 | 1.39 | 211.30 | 2.29 | 330 |
| 70 | 1.52 | 201.09 | 3.73 | 210 |
| 75 | 1.44 | 965.83 | 8.12 | 95 |
| 175 | 2.49 | 2.63 | 5.69 | 220 |
| 177 | 2.55 | 0.96 | 4.37 | 290 |
| 180 | 2.35 | 1.19 | 2.98 | 435 |
| 183 | 2.21 | 1.31 | 2.15 | 625 |
| 186 | 2.22 | 0.32 | 1.19 | 1030 |

where $Z$ is the temperature-dependent rate constant and $n$ the Avrami exponent whose value varies according to the crystallization mechanism. A normalized rate constant, $k = Z^{1/n}$, is usually evaluated for comparison purposes because its dimension

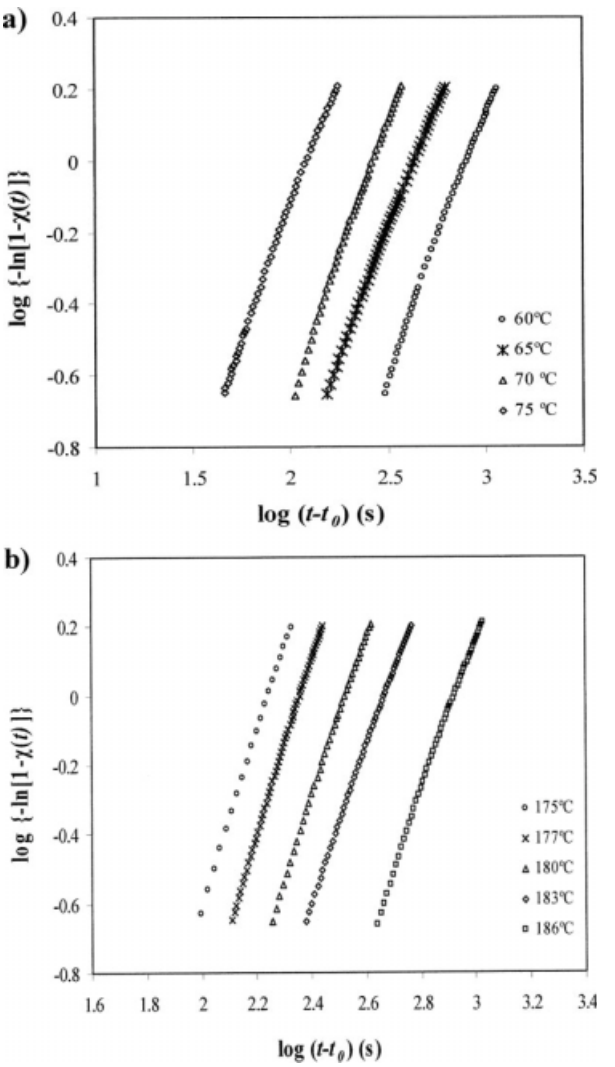


**Figure 11** (a) Avrami analyses for cold (a) and hot (b) isothermal crystallizations of PGL-P(GL-*co*-TMC)-PGL.

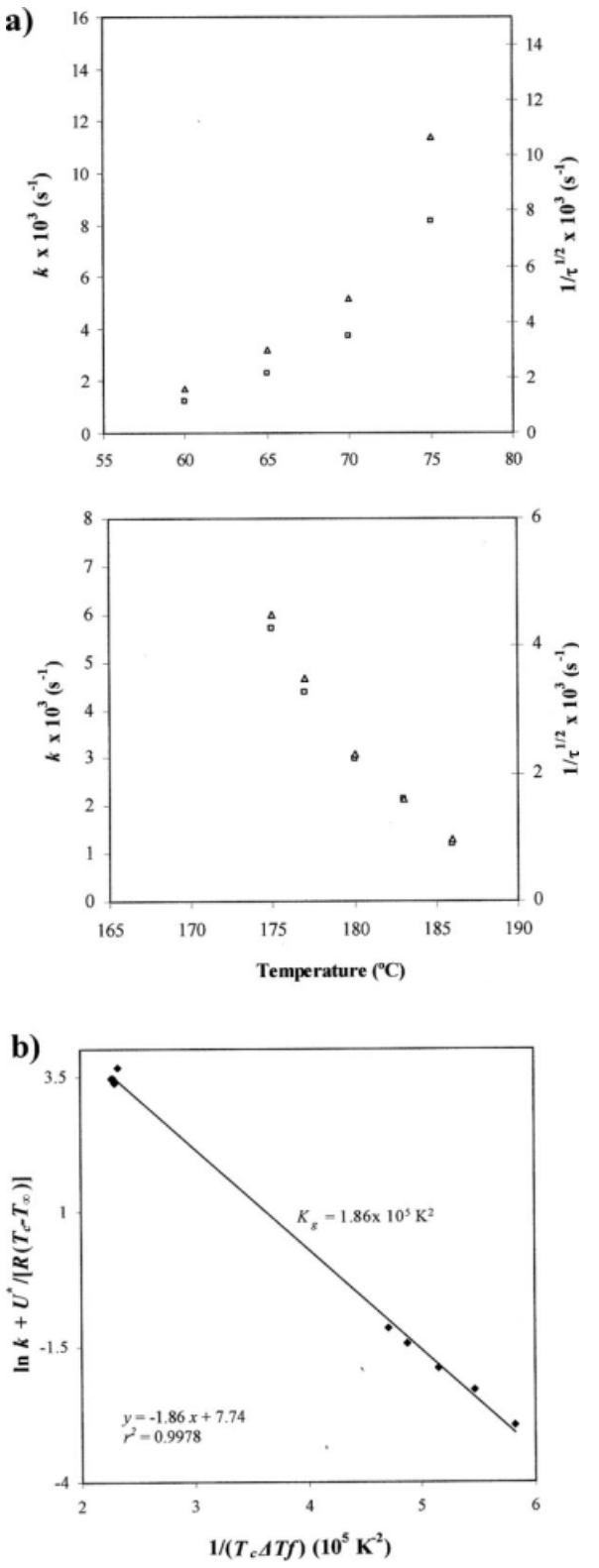


**Figure 12** (a) Overall crystallization rates (□) and the reciprocal of the crystallization half-times (△) determined at different temperatures for PGL-P(GL-*co*-TMC)-PGL samples. (b) Plot of ln $k + U^*/R$ $(T_c - T_\infty)$ versus $1/T_c(\Delta T)f$ to determine the secondary nucleation parameter of PGL-P(GL-*co*-TMC)-PGL.

(time$^{-1}$) is independent of the value of the Avrami exponent.

Table I summarizes the main kinetic parameters of the primary crystallization process, which were deduced from the plots of $\log\{-\ln[1 - \chi(t)]\}$ against $\log(t - t_0)$ (Fig. 11). The values of the Avrami exponent for the hot isothermal crystallizations lie in a narrow range, from 2.21 to 2.49, 2.36 being the average value. This suggests a predetermined (heterogeneous) nucleation with spherical growth that occurred under geometric constraints as the theoretical value should be equal to 3. Both sporadic (heterogeneous) and homogeneous nucleation can be clearly discarded as a higher exponent, close to 4,

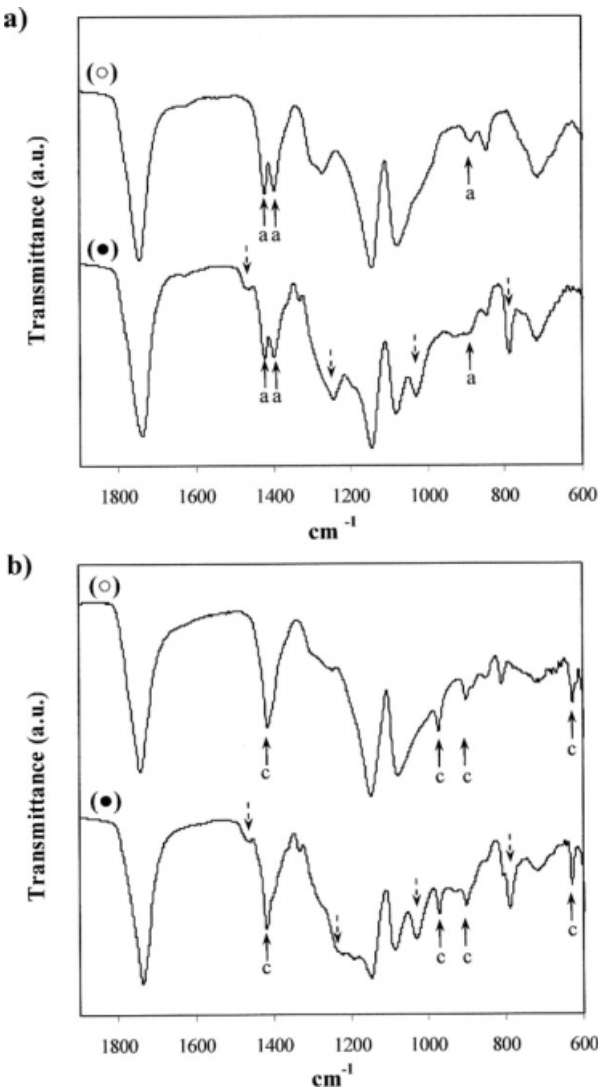


**Figure 13** Absorbance FTIR spectra (1900–600 cm$^{-1}$) of amorphous (a) and semicrystalline (b) PGL-P(GL-*co*-TMC)-PGL (●) and polyglycolide (○) samples. Characteristic bands of glycolide and trimethylene carbonate units are indicated by solid and dashed arrows, respectively. Labels a and c distinguish the bands associated with amorphous and crystalline phases, respectively.

**TABLE II**
**Representative Infrared Absorption Bands ($cm^{-1}$) Associated to the Amorphous and Crystalline Phases of Polyglycolide and the Amorphous Phase of Poly(trimethylene carbonate)[a]**

| | Trimethylene carbonate units | Glycolide units | |
|---|---|---|---|
| Assignment | Amorphous phase | Amorphous phase | Crystalline phase |
| $\delta$ $CH_2$ | 1468 m | 1460 m | |
| | | 1421 m | 1416 m |
| $\nu_{as}$ COC | 1221 vs | | |
| $\nu_s$ COC | 1090 m | | |
| $\nu$ C—C + $r$ $CH_2$ | | 897 m | 972 s |
| | | | 902 s |
| $\gamma$ C=O | 780 s | | 629 s |

[a] Abbreviations denote intensity or vibrational mode: vs, very strong; s, strong; m, medium; $\nu$, stretching; $\nu_{as}$, asymmetric stretching; $\nu_s$, symmetric stretching; $r$, rocking; $\gamma$, scissoring.

should be derived. Furthermore, a high undercooling is needed to favor a homogeneous nucleation.

Cold crystallization was characterized by a lower Avrami exponent because values ranged between 1.39 and 1.52 and the average value corresponded to 1.45. A predetermined nucleation should again be derived. However, in this case, geometric constraints are crucial.

The values of the corresponding crystallization half-times, calculated as the difference between the time at which crystallization begins and the time at which 50% of crystallization is completed, are also summarized in Table I. This parameter is a direct measure of the crystallization process and could therefore be used to check the accuracy of the Avrami analyses. In this way, Figure 12(a) shows a similar dependence of the reciprocal of the crystallization half-time, $1/\tau_{1/2}$, and the kinetic rate constant on the crystallization temperature, demonstrating the suitability of the deduced Avrami parameters.

Several reports have shown that the Hoffman and Lauritzen equation can be reformulated using the reciprocal crystallization half-time[26–28] ($1/\tau_{1/2}$), the reciprocal time to achieve a 5%[29] or a 25%[30] weight fraction crystallinity, or the normalized constant[31–34] ($k$) instead of the radial growth rate ($G$) when athermal nucleation is observed.

Specifically, we considered the derived equation for the normalized constant:

$$k = k_0 \exp[-U^*/(R(T_c - T_\infty))] \exp\left[-K_g/(T_c(\Delta T)f)\right]. \quad (4)$$

The corresponding LH plot in Figure 12(b) shows that the data fit with a straight line, which is indicative of a single crystallization regime. The values of $U^* = 1525$ cal/mol and $T_\infty = T_g - 35$ K as well as a nucleation constant of $1.86 \times 10^5$ $K^2$ were derived. Very good agreement is thus found between DSC and optical microscopy analyses.

Equation (4) and the estimated $U^*$, $T_\infty$, $K_g$, and $k_0$ parameters were used to determine the rate constant at different crystallization temperatures. The plot in Figure 8(b) shows the conventional bell-shaped curve expected from the interplay between segmental mobility and secondary nucleation. Good agreement is observed between the simulated curves obtained from DSC and optical microscopy data as the estimated crystallization parameters were very similar. This is unusual because the overall crystallization curve generally appears shifted to lower temperatures due to the influence of the primary nucleation rate.

Experimental crystallization studies on different polymers (e.g., poly(ethylene succinate)[35]) suggest that the primary nucleation rate exhibits a bell-shaped curve with crystallization temperature when crystallization follows a thermal nucleation process. The maximum nucleation rate is obtained at a lower temperature than that corresponding to the maximum growth rate, a trend that may account for the above shift between the curves corresponding to the overall rate constant and the growth rate. Recent experiments reported in the literature show that the primary nucleation step can be entirely completed by self-nucleating a polymer sample. In this case, the DSC data contain only contributions from crystal growth, and consequently, the curves corresponding to the overall crystallization rate constant and the growth rate should be similar.[36]

Isothermal crystallization of PGL-P(GL-*co*-TMC)-PGL is characterized by the fact that all primary nuclei become active when the exothermic crystallization peak starts to appear (i.e., after the induction time). In this way, a perfect match between the above curves should also be observed, clearly illustrating athermal nucleation. Implicitly, this demonstrates the

suitability of DSC analysis for determining the secondary nucleation parameter. Note, finally, that the above optical microscopy observations also suggest that all nuclei were active at the same time for a given crystallization temperature.

### FTIR spectroscopic analysis of the isothermal cold crystallization of PGL-P(GL-*co*-TMC)-PGL

FTIR is highly sensitive to molecular conformation and packing density, hence, its usefulness in polymer crystallization studies. Characteristic bands can be correlated to the crystalline and amorphous phases of the bulk and typically remain distinguishable over the course of crystallization. Isothermal studies are preferred to avoid shape susceptibility of FTIR bands with temperature. These studies are complementary to those performed by calorimetric techniques because they allowed deduction of kinetic parameters as a different kind of physical measures is considered.

Infrared bands due to glycolide units involved in crystalline and amorphous domains have been reported[37] and assigned considering accurate calculations performed with the polyglycine I structure,[38,39] which is a polyamide highly similar to polyglycolide. No amorphous samples could be prepared in this study, and the spectrum of amorphous polyglycolide was therefore computed by the difference between poly(D,L-lactide) and poly(D,L-lactide-*co*-glycolide) spectra.

We successfully obtained amorphous samples of polyglycolide by quenching the samples in liquid nitrogen and compared their spectra with those of semicrystalline samples (Fig. 13). Several FTIR bands could be clearly attributed to each phase; the observations being in full agreement with the reported data. Figure 13 also shows the spectra of amorphous and semicrystalline PGL-P(GL-*co*-TMC)-PGL samples. In this case, the TMC units should always belong to the amorphous phase, and consequently, the additional bands associated with these units appeared in both samples at the same wavenumber. Table II summarizes the main distinctive FTIR bands found in PGL-P(GL-*co*-TMC)-PGL samples.

To perform an accurate kinetic analysis, it is necessary to select intense and well-separated bands associated with crystalline or amorphous phases, which may be difficult due to the overlapping with TMC unit bands. FTIR bands observed at 972 and 902 $cm^{-1}$ were considered the most appropriate to follow the development of crystallinity. Figure 14(a) compares the absorbance spectra at the beginning and at the end of a cold crystallization performed at 64°C. These selected bands were assigned[37] to the crystalline phase of polyglycolide and specifically to highly coupled normal modes involving the skeletal $\nu_{CC}$ stretching and *r* $CH_2$ rocking.

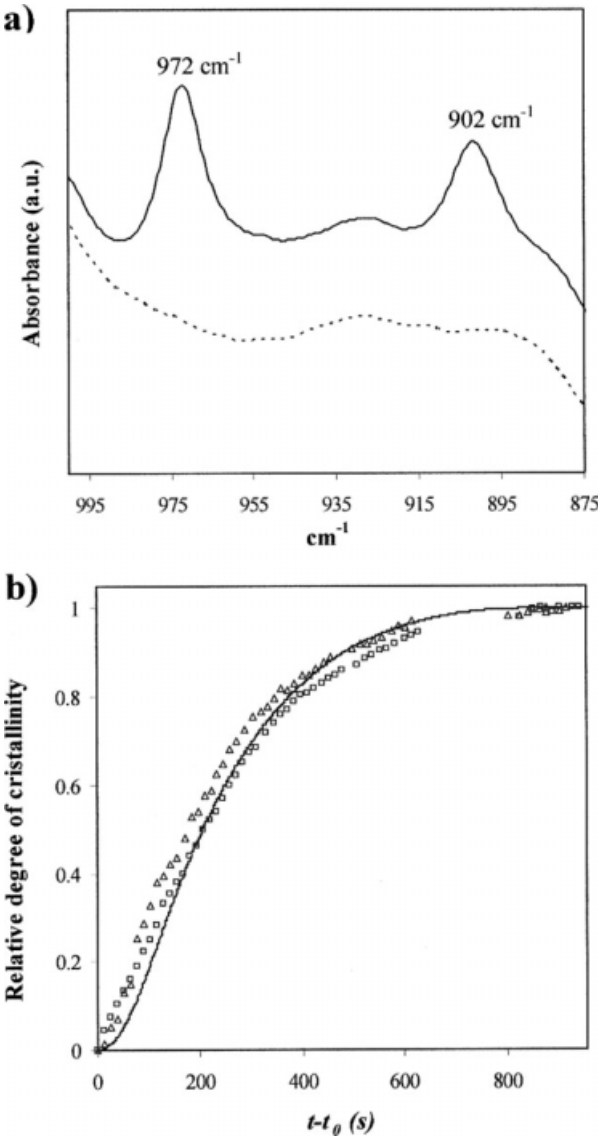


**Figure 14** (a) Absorption spectra (1000–875 $cm^{-1}$) of amorphous (dashed line) and semicrystalline (solid line) polyglycolide samples. (b) Development of crystallinity over time for the cold crystallization of PGL-P(GL-*co*-TMC)-PGL performed at 64°C, as deduced from absorbance measures of 972 (△) and 902 $cm^{-1}$ (□) bands. Calorimetric data for a crystallization performed at 70°C are also plotted (solid line) for comparative purposes.

A relative degree of crystallinity, $\chi(t)$, can be defined and measured for any of the absorption bands:

$$\chi(t) = (A_t - A_0)/(A_\infty - A_0), \quad (5)$$

where $A_t$ is the absorption measured at a crystallization time $t$, and $A_0$ and $A_\infty$ are the initial and final absorptions of the considered band, respectively.

Figure 14(b) compares the evolution of crystallinity, evaluated through absorption and DSC measurements for a representative temperature, whereas the kinetic parameters determined through Avrami

**TABLE III**
**Isothermal Cold Crystallization Kinetic Parameters Deduced from FTIR Experiments for the Segmented PGL-P(GL-*co*-TMC)-PGL Sample**

| $T_c$ (°C) | $n$ | $Z \times 10^5$ ($s^{-n}$) | $k \times 10^3$ ($s^{-1}$) | $\tau_{1/2}$ (s) |
|---|---|---|---|---|
| 61 | 1.19 | 100.2 | 3.09 | 250 |
| 64 | 1.22 | 103.4 | 3.65 | 207 |
| 66 | 1.23 | 119.8 | 4.24 | 175 |
| 69 | 1.29 | 210.9 | 8.48 | 85 |
| 71 | 1.31 | 341.0 | 12.97 | 55 |

analyses of FTIR data are summarized in Table III. Good agreement between FTIR and DSC experiments is found if a thermal lag close to 6°C is considered. Note that the Avrami exponents range between 1.19 and 1.31, again indicating that the cold crystallization process took place under strong geometric constraints.

## CONCLUSIONS

The hard and soft segments of PGL-P(GL-*co*-TMC)-PGL are completely miscible, and consequently, properties such as glass transition temperature become dependent on processing/crystallization conditions. Crystalline domains, which mainly correspond to polyglycolide hard segments, are susceptible to recrystallization/reorganization processes when a heating scan is performed. We found that thermal annealing may induce crystallization of highly defective crystals at a low melting temperature, which may be associated with the soft segment.

Hard polyglycolide segments crystallize from both the melt and the glass state as positive spherulites with a fibrillar texture. The unusual sign of birefringence of this polyester can be the result of its close packing structure, by which molecules with an all-trans conformation have an azimuthal orientation defined by a setting angle of 0°.

Crystallization occurs through an athermal primary nucleation, which allows determination of the secondary nucleation parameter by calorimetric analysis. Furthermore, crystallization is characterized by a low nucleation density. Thus, a study of the crystal growth rate can be conducted for the hot and cold crystallization processes by polarizing optical microscopy. We found that both techniques led to similar kinetic parameters and specifically to a secondary nucleation constant of 1.82–1.86 $\times 10^5$ $K^2$.

Cold crystallization occurs under stronger geometric constraints than hot crystallization, as deduced from the decrease of the Avrami exponent (from 2.32 to 1.45). The results obtained from FTIR analysis for the cold crystallization are in full agreement with DSC measurements and indicate again a low value for the Avrami exponent.

The authors express their gratitude to B. BRAUN Surgical S. A. for the collaboration and support.

## References

1. Frazza, E. J.; Schmitt, E. E. J Biomed Mater Res Symp 1971, 1, 43.
2. Athanasiou, K. A.; Agrawal, C. M.; Barber, F. A.; Burkhart, S. S. Arthroscopy 1998, 14, 726.
3. Middleton, J. C.; Tipton, A. J. Biomaterials 2000, 21, 2335.
4. Buchholz, B. J. J Mater Sci: Mater Med 1993, 4, 381.
5. Hurrel, S.; Cameron, R. E. Biomaterials 2002, 23, 2401.
6. Wang, Z. G.; Hsiao, B. S.; Zong, X.; Yeh, F.; Zhou, J. J.; Dormier, E.; Jamiolkowski, D. D. Polymer 2000, 41, 621.
7. Fu, B. X.; Hsiao, B. S.; Chen, G.; Zhou, J.; Lin, S.; Yuan, J.; Koyfman, I.; Jamiolkowsky, D. D.; Dormier, E. Chin J Polym Sci 2003, 21, 159.
8. Zong, X.; Ran, S.; Fang, D.; Hsiao, B. S.; Chu, B. Polymer 2003, 44, 4959.
9. Hill, S.; Montes de Oca, H.; Klein, P.; Ward, I.; Rose, J.; Farrar, D. Biomaterials 2006, 27, 3168.
10. Bezwada, R. S.; Jamiolkowski, D. D.; Lee, I. Y.; Agarwal, V.; Persivale, J.; Trenka-Bethin, S.; Erneta, M.; Persivale, J.; Suryadevara, J.; Yang, A.; Liu, S. Biomaterials 1995, 16, 1141.
11. Hoffman, J. D.; Weeks, J. J. J Chem Phys 1962, 37, 1723.
12. Lebedev, B. V.; Yepstropov, A. A.; Kiparisova, V. G.; Belov, V. I. Polym Sci USSR 1978, 113, 32.
13. Takayanagi, M.; Yamashita, T. J Polym Sci 1956, 22, 552.
14. Chatani, Y.; Suehiro, K.; Okita, Y.; Tadokoro, H.; Chujo, K. Makromol Chem 1968, 113, 215.
15. Furuhashi, Y.; Iwata, T.; Sikorski, P.; Atkins, E.; Doi, Y. Macromolecules 2000, 33, 9423.
16. Bunn, C. W.; Garner, E. V. Proc R Soc London Ser A 1947, 189, 39.
17. Lovinger, A. J. J Appl Phys 1978, 49, 5003.
18. Lovinger, A. J. J Appl Phys 1978, 49, 5014.
19. Lauritzen, J. I.; Hoffman, J. D. J Appl Phys 1973, 44, 4340.
20. Strobl, G. Eur Phys J 2000, 3, 165.
21. Muthukumar, M. Eur Phys J 2000, 3, 199.
22. Williams, M. L.; Landel, R. F.; Ferry, J. D. J Am Chem Soc 1955, 77, 3701.
23. Suzuki, T.; Kovacs, A. J. Polym J 1970, 1, 82.
24. Avrami, M. J Chem Phys 1939, 7, 1103.
25. Avrami, M. J Chem Phys 1940, 8, 212.
26. Philips, P. J.; Lambert, W. S. Macromolecules 1990, 23, 2075.
27. Urbanovici, E.; Schneider, H. A.; Cantow, H. J. J Polym Sci Part B: Polym Phys 1997, 35, 359.
28. Hong, P. D.; Chung, W. T.; Hsu, C. F. Polymer 2002, 43, 3335.
29. Heberer, D. P.; Cheng, S. Z. D.; Barley, J. S.; Lien, S. H. S.; Bryant, R. G.; Harris, F. W. Macromolecules 1991, 24, 1890.
30. Lu, X. F.; Hay, J. N. Polymer 2001, 42, 9423.
31. Chan, T. W.; Isayev, A. I. Polym Eng Sci 1994, 34, 461.
32. Fatou, J. G.; Marco, C.; Mandelkern, L. Polymer 1990, 31, 890.
33. Lu, H.; Qiao, J.; Yang, Y. Polym Int 2002, 51, 1304.
34. Kenny, J. M.; Maffezzoli, A.; Nicolais, R. Thermochim Acta 1993, 227, 83.
35. Umemoto, S.; Hayashi, R.; Kawano, R.; Kikutani, T.; Okui, N. J Macromol Sci Phys 2003, 42, 421.
36. Lorenzo, A. T.; Müller, A. J. J Polym Sci Part B: Polym Phys 2008, 46, 1478.
37. Kister, G.; Cassanas, G.; Vert, M. Spectrochim Acta Part A 1997, 53, 1399.
38. Abe, Y.; Krimm, S. Biopolymers 1972, 11, 1817.
39. Moore, W. H.; Krimm, S. Biopolymers 1976, 15, 2439.